Aalborg Universitet

AALBORG UNIVERSITY
DENMARK

Design and Experimental Validation of Automated Millimeter-Wave Phased Array Antenna-in-Package (AiP) Experimental Platform

Gao, Huaqiang; Wang, Weimin; Fan, Wei; Zhang, Fengchun; Wang, Zhengpeng ; Wu, Yongle ; Liu, Yuanan; Pedersen, Gert Frølund

Published in:
I E E E Transactions on Instrumentation and Measurement

DOI (link to publication from Publisher):
10.1109/TIM.2020.3024428

Publication date:
2020

Document Version
Accepted author manuscript, peer reviewed version

Link to publication from Aalborg University

Citation for published version (APA):
Gao, H., Wang, W., Fan, W., Zhang, F., Wang, Z., Wu, Y., Liu, Y., & Pedersen, G. F. (2020). Design and Experimental Validation of Automated Millimeter-Wave Phased Array Antenna-in-Package (AiP) Experimental Platform. *I E E E Transactions on Instrumentation and Measurement*, *70*, Article 9199297. https://doi.org/10.1109/TIM.2020.3024428

General rights
Copyright and moral rights for the publications made accessible in the public portal are retained by the authors and/or other copyright owners and it is a condition of accessing publications that users recognise and abide by the legal requirements associated with these rights.

- Users may download and print one copy of any publication from the public portal for the purpose of private study or research.
- You may not further distribute the material or use it for any profit-making activity or commercial gain
- You may freely distribute the URL identifying the publication in the public portal -

Take down policy
If you believe that this document breaches copyright please contact us at vbn@aub.aau.dk providing details, and we will remove access to the work immediately and investigate your claim.

This article has been accepted for publication in a future issue of this journal, but has not been fully edited. Content may change prior to final publication. Citation information: DOI 10.1109/TIM.2020.3024428, IEEE Transactions on Instrumentation and Measurement

Design and Experimental Validation of Automated Millimeter-Wave Phased Array Antenna-in-Package (AiP) Experimental Platform

Huaqiang Gao, Weimin Wang, Wei Fan, Fengchun Zhang, Zhengpeng Wang, Yongle Wu, Yuanan Liu, and Gert Frølund Pedersen

***Abstract*—Antenna-in-package (AiP) technology has been a main design scheme of millimeter-wave (mmWave) phased array antennas for 5G communications. The beamforming pattern of mmWave phased array AiP is steered by controlling the amplitude and phase excitations of AiP elements. It would be helpful to evaluate the control accuracy of complex excitations and to reliably calibrate mmWave AiP. However, these tasks are not trivial and time-consuming in practice, especially when the number of AiP elements is large. To address this problem, this paper presents an efficient and automated mmWave phased array experimental platform. To reduce measurement time, a control software is developed to automatically control the AiP and measurement instruments simultaneously. This experimental platform has flexible gain and phase control of AiP element excitations, and customized measurements in an automated and efficient way can be realized. The effectiveness of the experimental platform is demonstrated by several measurement campaigns, where control accuracy, array calibration, and beam steering for mmWave phased array AiP are extensively investigated.**

***Index Terms*—5G, millimeter-wave (mmWave) antenna-in-package (AiP), phased array calibration, control accuracy, experimental platform.**

I. Introduction

WITH the expeditious evolution of wireless mobile telecommunication technology from 1G to 5G, millimeter-wave (mmWave) frequency band has attracted significant research interest in terms of the high throughput and low latency in recent years [1], [2]. At the mmWave frequencies, the antenna dimension is reduced to millimeters. Such miniaturized antennas make the integration design possible. As an important antenna and packaging solution for mmWave applications over the years, antenna-in-package (AiP) technology integrates antennas and radio frequency integrated circuits (RFICs) in a single package to achieve system-level wireless functions [3]–[6]. AiP design is currently the main solution for mmWave smartphone antennas due to its advantages of miniaturization, low cost and simplicity, etc. With modular designing of AiPs, scalable mmWave phased arrays are extensively applied in terms of beamforming and directional links for cellular and satellite communications [7]. Phased array AiPs offer spatial discrimination capability for target and interfering signals in the far field region, via controlling the complex excitation of individual antenna elements.

Much work on the mmWave phased array AiP was reported in the literature. For example, a mmWave phased array IC with dual polarizations and beam steering control is demonstrated in [8], where the performance of different mmWave silicon-based packaged phased arrays were compared. Reference [9] presented a mmWave phased array AiP with stamped metal. The heat emission generated from the RFICs in the AiP was effectively dissipated. A miniaturized mmWave wideband dual-polarized AiP array was designed for cellular phones in [10]. The relevant simulation results are presented for the licensed 5G cellular bands. The focus of the reported work is mostly on the IC and antenna design of mmWave AiPs.

However, extensive evaluation of the control error and array calibration for mmWave phased array AiP after integration is still challenging in practice [11], [12]. The gain and phase control of AiP element excitations is achieved in AiP chips. The relative deviation exists between the desired control setting and the practical output of control, i.e. the control error or accuracy [13], [14]. This control accuracy affects the AiP performance. For mmWave mobile terminal antenna design, the main beam is the main focus (i.e. main beam spatial/angular coverage area and associated gain level), while other metrics, e.g. side-lobes and nulls are also required for some applications, e.g. mmWave base station. Therefore, it would be meaningful to understand the control error of the mmWave AiP, i.e. to what extent the accuracy of the AiP control is achieved in practical setup. Furthermore, AiP control accuracy differs, depending on whether AiP elements are active or disabled. This is mainly due to the AiP design and antenna coupling. This study is, however, largely overlooked in the literature.

On the other hand, initial excitation differs among AiP elements in practical design. The AiP is calibrated by compensating for the initial excitation differences among AiP elements obtained by calibration measurement [15], to ensure reliable AiP performance. The research question is how to reliably

This work was supported by Beijing Natural Science Foundation (No. JQ19018), National Natural Science Foundations of China (No. 61701041, 61971052, and No. 61821001). (Corresponding author: Weimin Wang, Wei Fan, and Yongle Wu.)

Huaqiang Gao, Weimin Wang, Yongle Wu, and Yuanan Liu are with the Beijing Key Laboratory of Work Safety Intelligent Monitoring, Department of Electronic Engineering, Beijing University of Posts and Telecommunications, Beijing 100876, China (e-mail: gaohq@ieee.org; wangwm@bupt.edu.cn; wuyongle138@gmail.com; and yuliu@bupt.edu.cn).

Wei Fan, Fengchun Zhang, and Gert Frølund Pedersen are with the Antenna Propagation and Millimeter-wave Systems (APMS) section, Department of Electronic Systems, Faculty of Engineering and Science, Aalborg University, Aalborg 9220, Denmark (e-mail: wfa@es.aau.dk; fz@es.aau.dk; gfp@es.aau.dk).

Zhengpeng Wang is with the Electronics and Information Engineering, Beihang University, Beijing 100191, China (e-mail: wangzp@buaa.edu.cn).

0018-9456 (c) 2020 IEEE. Personal use is permitted, but republication/redistribution requires IEEE permission. See http://www.ieee.org/publications_standards/publications/rights/index.html for more information.
Authorized licensed use limited to: Aalborg Universitetsbibliotek. Downloaded on October 01,2020 at 12:59:20 UTC from IEEE Xplore. Restrictions apply.

This article has been accepted for publication in a future issue of this journal, but has not been fully edited. Content may change prior to final publication. Citation information: DOI 10.1109/TIM.2020.3024428, IEEE Transactions on Instrumentation and Measurement

calibrate the mmWave phased array AiP? The array calibration can be typically done in the near field scanning calibration measurement, where probe antenna is placed in front of each and every array element and the element excitation differences are recorded. However, the accurate mechanical positioning is difficult, and phase measurement accuracy is challenging at mmWave band. The far field "on-off" calibration, i.e. probe placed in the far field to record element excitation difference via the "on-off" operation of elements, would be more promising for the miniaturized AiP with limited far-field distance. However, it is unclear whether the "on-off" operation would cause inaccurate calibration results. This paper attempts to address the above-mentioned issues, and investigates the control accuracy and calibration measurement of a mmWave phased array AiP. To the best of our knowledge, very limited work on this has been addressed in the literature.

In this paper, an automated mmWave phased array AiP experimental platform is developed to quickly and efficiently perform the control accuracy and calibration measurement of a mmWave phased array AiP. The AiP experimental platform is composed of hardware configuration and control software. Specifically, this platform has the following merits:

1) Individual control of AiP elements, including Tx/Rx switch, on/off switch, attenuation and phase shift. For the commerically available mmWave phased array AiP [16], typically only beamforming mode is supported, i.e. phases of elements are controlled together according to the impinging angle. However, full flexibility to individually control the element amplitude and phase is typically not available.
2) Automatic and customized measurements, including control accuracy, array calibration, and beam steering. The measurement results will help engineers and researchers to understand the performance of the mmWave phased array AiP. This is not possible if an automated platform is not available due to the large amount of required measurements and long measurement time.
3) Research and development support for various mmWave applications, e.g. phased array calibration, beamforming and nulling operation, array pattern synthesis, beam pattern side-lobe suppression with tapering algorithms, and plane wave generator, etc.

The rest of this paper is organized as follows. Section II describes the hardware configuration of the mmWave phased array AiP experimental platform, followed by the corresponding software control framework in Section III. To evaluate the performance of the AiP experimental platform, in Section IV, extensive measurements are conducted with measurement instrument, e.g. the network analyzer. Finally, conclusions are presented in Section V.

II. Hardware Configuration

The hardware part of the experimental platform is a 4×4 phased array AiP module from Amotech Co., Ltd. [17]. The photograph and the structure diagram of the 4×4 AiP module are illustrated in Fig. 1. The AiP module consists of a AiP board with a 4×4 AiP, a microprogrammed control unit

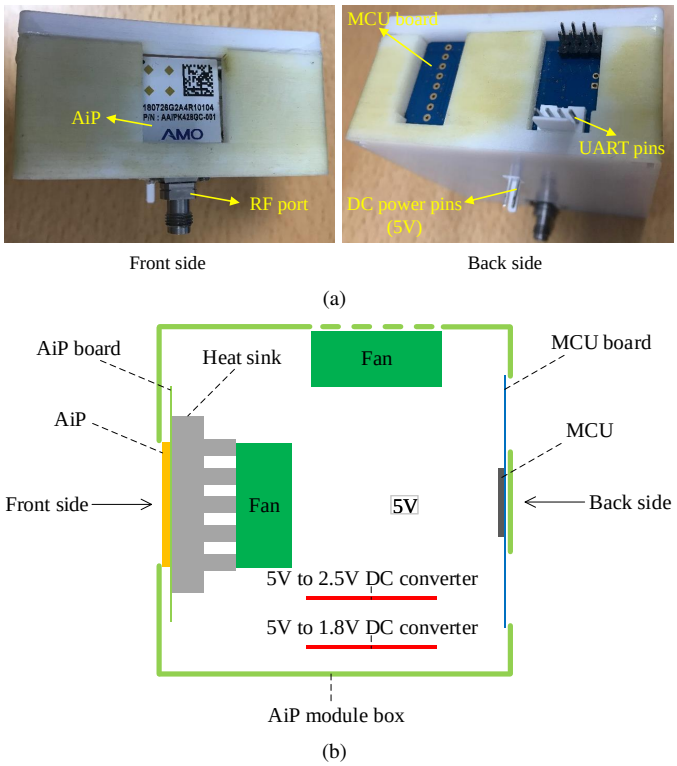

Fig. 1. Photograph (a) and structure diagram (b) of the AiP module.

(MCU) board with a MCU (STM32F427VIT6), a heat sink, two fans, and two DC converters. The heat sink and fans are used for the cooling of AiP chipset, and two DC converters (1.8 V and 2.5 V) are for the dual supply. The 4×4 AiP and the MCU are two major components of the AiP module, which are explained separately below.

The 4×4 AiP integrates 4 RFICs (AWMF-0158 chipset) with 16 patch antennas into a package. As a silicon quad core IC (operating from 26.5 to 29.5 GHz), each AWMF-0158 chip supports 4 transmit(Tx)/receive(Rx) radiating elements in half duplex mode [18]. The block diagram of the 4×4 AiP is demonstrated in Fig. 2. For Tx or Rx mode selected by switch, the AiP has individual gain (attenuation) and phase control chain for each element. Each control chain incorporates an attenuator (called element attenuator in the following), a phase shifter, and an amplifier. The amplifier is a power amplifier (PA) or a low noise amplifier (LNA), which are for Tx or Rx modes, respectively. The PA and the LNA are turned on when Tx mode and Rx mode are enabled, respectively. Simultaneously, the amplifier has power down function for each element. Besides the individual control chain, the AiP has another two common attenuators and two temperature variable attenuators (TVA) for four elements in each chip. The element attenuator has an attenuation resolution of 0.5 dB for each single element, while the common attenuator has an attenuation resolution of 1 dB for the entire chip. The phase shifters with 6 bits have a least significant bit (LSB) of $360/2^6 = 5.625°$. Fig. 3 exhibits the antenna view of the AiP. The side length of square AiP and the element spacing is 21.8 mm and 5.45 mm (0.51 λ at 28 GHz), respectively.

0018-9456 (c) 2020 IEEE. Personal use is permitted, but republication/redistribution requires IEEE permission. See http://www.ieee.org/publications_standards/publications/rights/index.html for more information.
Authorized licensed use limited to: Aalborg Universitetsbibliotek. Downloaded on October 01,2020 at 12:59:20 UTC from IEEE Xplore. Restrictions apply.

This article has been accepted for publication in a future issue of this journal, but has not been fully edited. Content may change prior to final publication. Citation information: DOI 10.1109/TIM.2020.3024428, IEEE Transactions on Instrumentation and Measurement

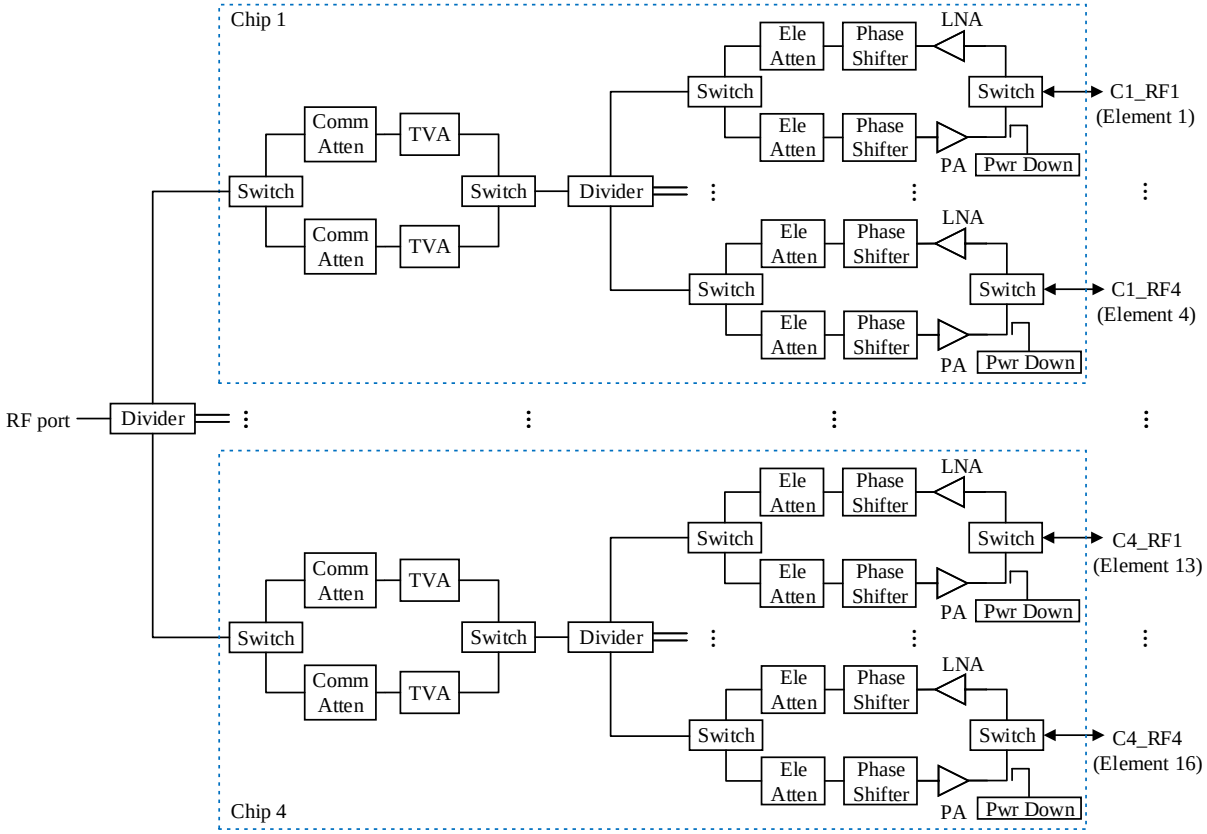

Fig. 2. Block diagram of the AiP.

The MCU receives commands from the upper computer (e.g. laptop) by universal asynchronous receiver/transmitter (UART) serial communication. The commands are parsed, judged, and then processed accordingly (e.g. controlling AiP through serial peripheral interface). Finally, the corresponding processing result is returned to the upper computer.

III. Software Control

A homemade control software is developed for the AiP module using C++ language and Qt framework. The software interface is displayed in Fig. 4. Three main parts in the software interface are introduced below.

1) Individual Control of Elements: The on/off switch, attenuation and phase shift are set for each element in the software interface. The element layout in the software interface is the same as the antenna view in Fig. 3.

2) Beam Tilting Control: Based on the individual control of elements above, the phase shift between elements is set for the tilting of the main beam. The broadside direction of AiP is denoted as angle 0°. The main beam can be tilted leftwards, rightwards, forwards, and backwards with respect to the broadside direction, by setting the phase difference between elements. The phase difference between element columns is set for the leftward and rightward tilting, while the phase difference between element rows is set for forward and backward tilting.

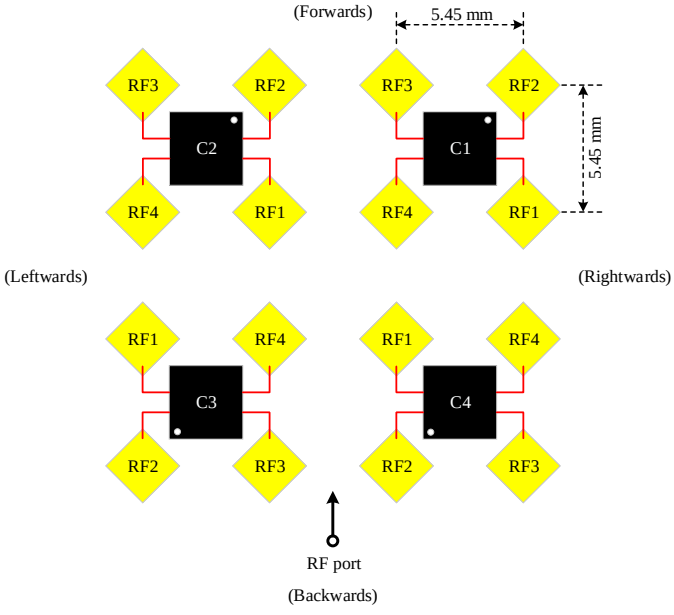

Fig. 3. Antenna view of the AiP.

3) Automatic and Customized Measurement: This part implements the automatic software control for the customized measurement items in the following measurement campaign. The measurement instrument is a vector network analyzer (VNA). The measurement items cover control accuracy, array

0018-9456 (c) 2020 IEEE. Personal use is permitted, but republication/redistribution requires IEEE permission. See http://www.ieee.org/publications_standards/publications/rights/index.html for more information.
Authorized licensed use limited to: Aalborg Universitetsbibliotek. Downloaded on October 01,2020 at 12:59:20 UTC from IEEE Xplore. Restrictions apply.

This article has been accepted for publication in a future issue of this journal, but has not been fully edited. Content may change prior to final publication. Citation information: DOI 10.1109/TIM.2020.3024428, IEEE Transactions on Instrumentation and Measurement

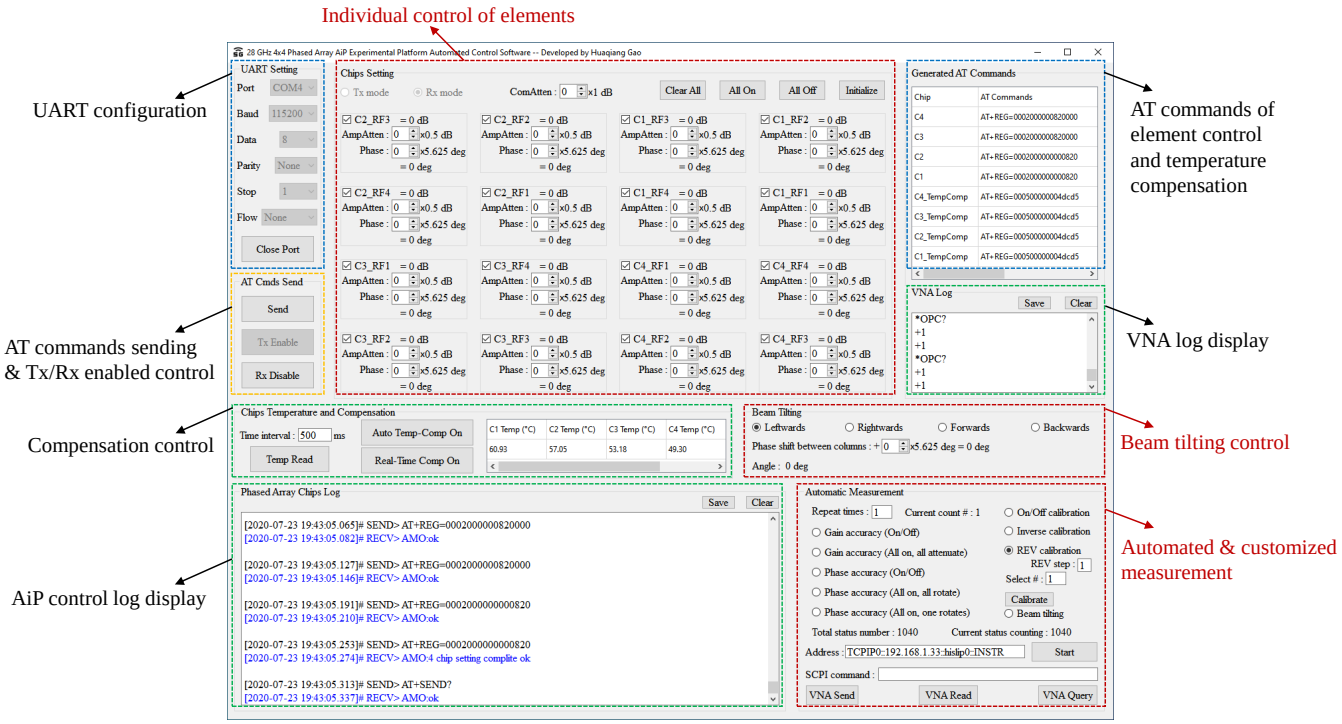

Fig. 4. Software interface of AiP experimental platform.

calibration, and beam steering measurement. In each measurement item, the status of AiP (i.e. on/off, attenuation, and phase shift) is constantly updated by AiP control. After the status of AiP is updated, one measurement is conducted and data is saved by VNA control. The AiP control and VNA control are repeated in order until all status and data are updated and saved, respectively.

IV. Measurement Campaign

A. Measurement Setup

In order to evaluate the performance and to validate the effectiveness of the mmWave phased array AiP experimental platform, a measurement campaign was carried out in an anechoic chamber. As illustrated in Fig. 5, the measurement setup consists of the following components:

1) A phased array AiP module;
2) A standard gain horn (SGH) of model 22240-20, with a wide frequency band ranging from 26.4 to 40.1 GHz;
3) A VNA of model N5227A with the frequency range from 10 MHz to 67 GHz;
4) A 5V DC power supply for the AiP module;
5) A laptop for the control of AiP module and VNA using a USB to UART cable and a LAN cable, respectively;
6) An anechoic chamber;
7) Absorbers to cover the mmWave AiP and SGH antenna. Note that the antennas are buried in the absorbers and therefore not shown in Fig. 5(a).

The SGH points to the broadside of AiP. The aperture center of SGH is aligned with that of AiP vertically by two positioning lasers. Meanwhile, the AiP or SGH antenna is rotated horizontally. The relative position of the two antennas is not fixed until the maximal transmission power is measured by VNA to ensure that the polarization of the AiP and SGH is aligned as well. The alignment of the two antennas is demonstrated in Fig. 6. The distance between them is 730 mm, which is larger than the far field distance of both AiP and SGH. VNA ports 3 and 4 are connected to the SGH port and the AiP port (RF port of AiP module), respectively. The RF cables between SGH and AiP ports are calibrated applying the short-open-load-through (SOLT) calibration method by an electronic calibration kit (Keysight N4692-60001). The complex S-parameter S_{43} or S_{34} is measured in Rx or Tx mode of AiP, respectively. The VNA setting is as follows:

1) The frequency is swept from 26.5 to 29.5 GHz, with 3001 frequency points for multipath analysis. For the S-parameters measurement at 28 GHz, the frequency is set to 28 GHz with 1 frequency point.
2) The power level is set to 5 dBm;
3) The intermediate frequency (IF) bandwidth is set to 1 kHz.

Since the SGH is passive and the AiP is active, the performance (e.g. status change) of any RF components in the AiP (including attenuators, phase shifters, PAs, LNAs, etc.) is reflected in the complex S_{43} or S_{34}.

1) Multipath Analysis: First of all, the propagation channel between the SGH and the AiP is investigated. This is to ensure that only the line-of-sight (LOS) path exists between the SGH and AiP. The measurement results, e.g. array calibration can be affected if multipath exists. Taking the Rx mode of AiP for example, the measured channel frequency response (CFR) and channel impulse response (CIR) from SGH port to AiP port are given in Fig. 7. The CIR is obtained by applying the inverse

0018-9456 (c) 2020 IEEE. Personal use is permitted, but republication/redistribution requires IEEE permission. See http://www.ieee.org/publications_standards/publications/rights/index.html for more information.
Authorized licensed use limited to: Aalborg Universitetsbibliotek. Downloaded on October 01,2020 at 12:59:20 UTC from IEEE Xplore. Restrictions apply.

This article has been accepted for publication in a future issue of this journal, but has not been fully edited. Content may change prior to final publication. Citation information: DOI 10.1109/TIM.2020.3024428, IEEE Transactions on Instrumentation and Measurement

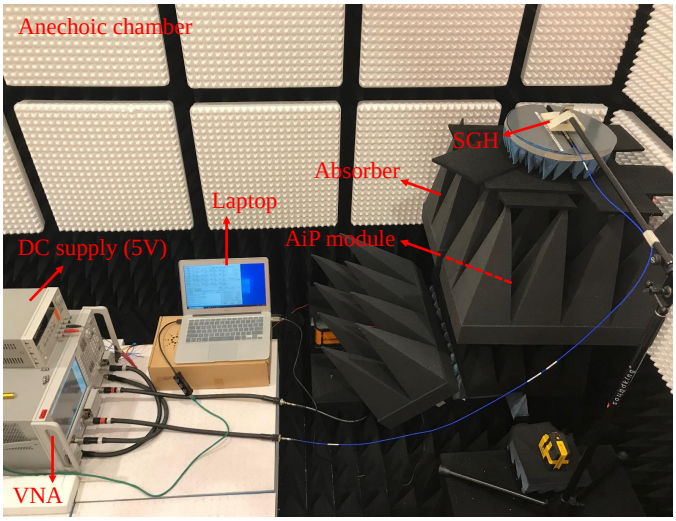

(a)

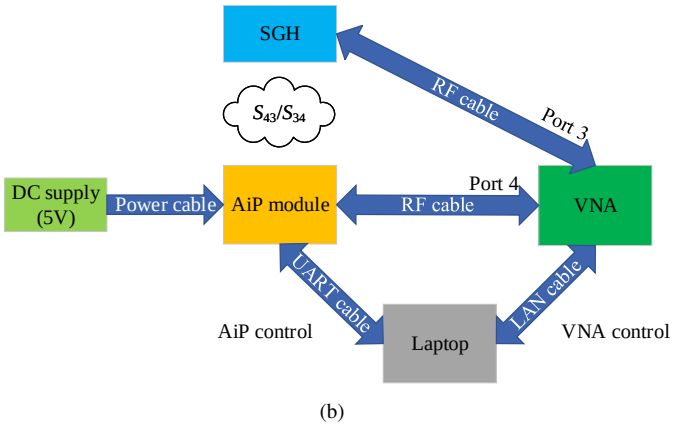

(b)

Fig. 5. Photograph (a) and block diagram (b) of the measurement setup in an anechoic chamber.

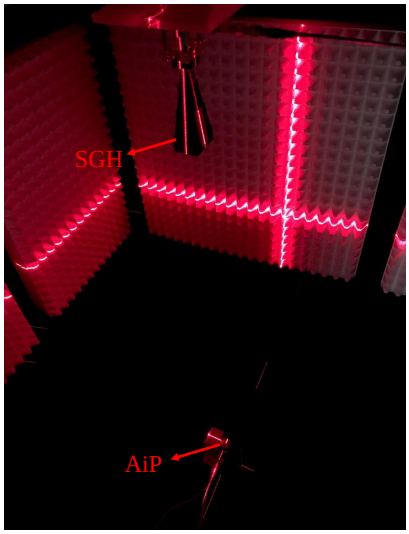

Fig. 6. Alignment of the mmWave AiP and the SGH antenna in an anechoic chamber.

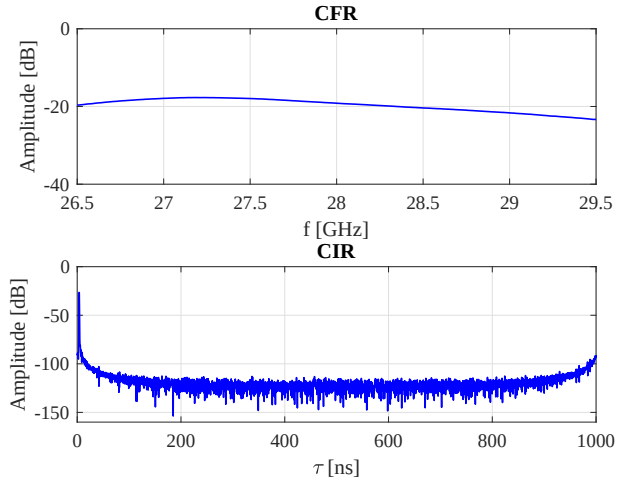

Fig. 7. Measured CFR (S_{43} with frequency range from 26.5 to 29.5 GHz) and CIR of the channel between SGH port and AiP port.

Fourier transform of CFR with the frequency range from 26.5 to 29.5 GHz. Obviously, only one single LOS path is observed from the CIR curve. Therefore, the channel between the SGH and the AiP is considered as a single path environment. If multiple paths exist in the channel in practical measurement environment, the CFR for single path channel is obtained by applying post-processing time gating algorithms to the original CIR. In addition, the LOS path appears at the delay of 3.67 ns. Since the distance between the SGH and the AiP is 0.73 m where the delay is 2.44 ns, the extra delay of 1.23 ns might be caused by the signal propagation in the SGH and the AiP.

2) Tx/Rx Stability Measurement: Before the following measurement, the stability of AiP is evaluated in both Rx and Tx modes. The chip temperature is affected by the on and off of PAs and LNAs, and in turn impacts the power output of PAs and LNAs. The power output does not become stable until the chip temperature is stable because the gain of the amplifier varies with the temperature. Fig. 8 shows the S-parameter amplitude and average chip temperature varied with operating time in both Rx and Tx modes. The amplitude becomes stable after Rx and Tx modes are enabled for 5 minutes and 9 minutes, respectively. The average chip temperature has the similar tendency. The Rx mode has faster stability than Tx mode. The amplitude decline with a range of 1.1 dB in Rx mode, and 4.5 dB in Tx mode, respectively. The average chip temperature increases from 35 °C to 60 °C and 100 °C in Rx mode and Tx mode, respectively. The Tx mode has a larger declining range of amplitude from start to stability than the Rx mode because of larger temperature change.

In addition, we attempt to apply two compensation operations for the Tx mode to reduce the amplitude declining range before stability. The first method is to adopt the feature of gain compensation over temperature in the AiP chipset (called the temperature compensation method in the following). On the basis of the chip temperature read from the AiP chipset, the corresponding commands of temperature compensation is sent to the MCU. The second method (called the custom compensation method) is to read measured S_{34} amplitude value from VNA at certain time intervals, and to compare this amplitude value with the initial one. Whenever the amplitude difference is beyond a certain value, the attenuation of chips

0018-9456 (c) 2020 IEEE. Personal use is permitted, but republication/redistribution requires IEEE permission. See http://www.ieee.org/publications_standards/publications/rights/index.html for more information.
Authorized licensed use limited to: Aalborg Universitetsbibliotek. Downloaded on October 01,2020 at 12:59:20 UTC from IEEE Xplore. Restrictions apply.

This article has been accepted for publication in a future issue of this journal, but has not been fully edited. Content may change prior to final publication. Citation information: DOI 10.1109/TIM.2020.3024428, IEEE Transactions on Instrumentation and Measurement

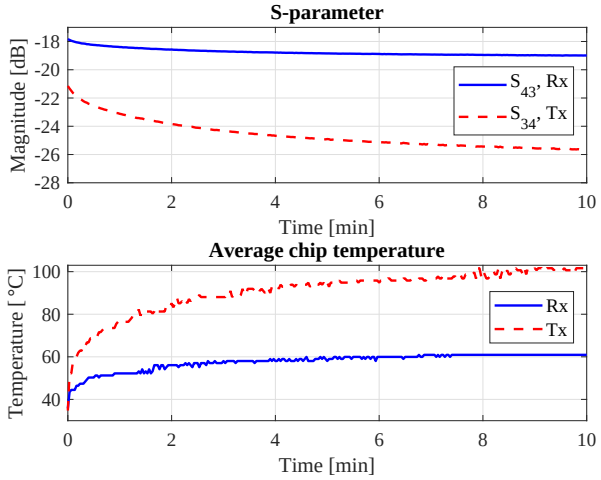

Fig. 8. S-parameter amplitude and average chip temperature over time in both Rx and Tx modes.

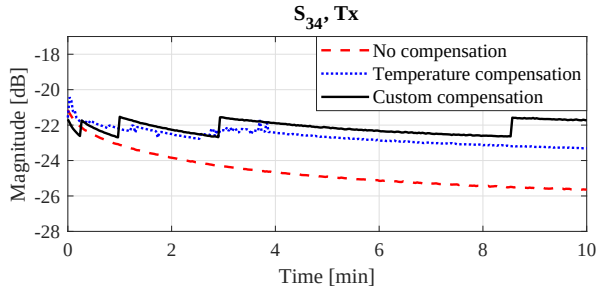

Fig. 9. S_{34} amplitude over the operating time with and without compensation in Tx mode of AiP.

is reduced by that value in the common attenuator (e.g. 1 dB). The S_{34} amplitude over time is displayed in Fig. 9 with and without compensation. With the temperature compensation method, the amplitude basically fluctuates within a range of 1.5 dB. The amplitude is stable within a fluctuation range of 1 dB with the custom compensation method. The custom compensation operation is unnecessary after the AiP is stable. However, if a non-negligible drift of amplitude exists over a long time, the custom compensation method still works. Otherwise, the requisite measurements must be completed within a certain period of time during which the AiP is considered as stable for the measurements. The Rx mode of AiP is adopted for the following measurement.

B. Control Accuracy

In this part, the practical attenuation and phase shift are validated when desired attenuation and phase shift are set in the AiP. The relative deviation of measured output offset (output value x) with respect to desired setting offset (target value a) is defined as the control error or accuracy. The control accuracy reflects the error introduced by the digital attenuator and phase shifters in the AiP. Depending on the mmWave AiP application, the control error of attenuators (gain control accuracy) and phase shifters (phase control accuracy)

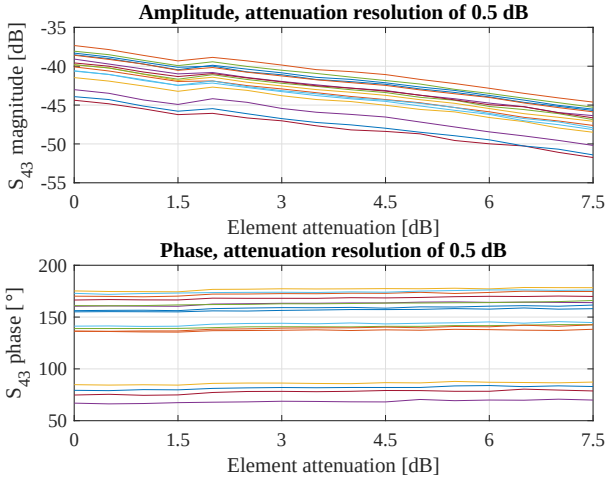

Fig. 10. Complex S_{43} as a function of the element attenuation in the "on-off" mode. 16 curves stand for 16 elements.

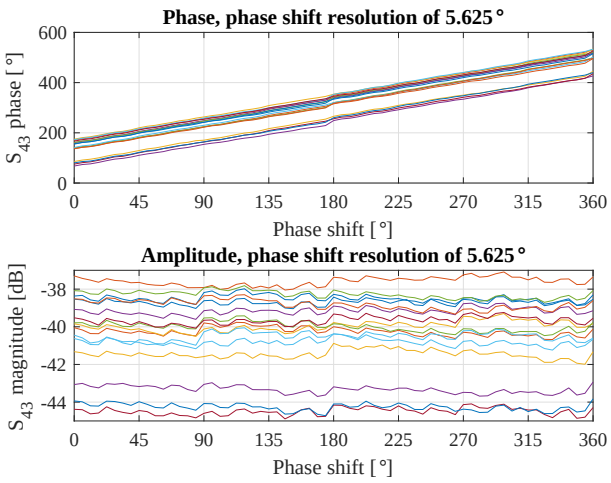

Fig. 11. Complex S_{43} as a function of the phase shift in the "on-off" mode. 16 curves stand for 16 elements.

is evaluated in two modes separately, i.e. "on-off" and "all-on" modes.

1) "On-off" Mode: In the "on-off" mode, only one element is sequentially enabled each time. The phase shift of the selected element is set to 0° in the gain control accuracy measurement. The attenuation of element attenuator is swept from 0 to 7.5 dB with a resolution step of 0.5 dB (i.e. a total of 16 measurements for $M = 16$ attenuation values). The complex S_{43} with the element attenuation increasing is presented in Fig. 10. The amplitude declines while the phase drifts with attenuation. The relative deviation of measured S_{43} amplitude increment x between every two adjacent attenuation values with respect to the gain setting offset $a = -0.5$ dB is defined as the gain control error (i.e. absolute error $\varepsilon = x - a$). The maximum error range among elements is $[\varepsilon|_{\min}, \varepsilon|_{\max}] = [-0.4, 1.2]$ dB. The corresponding root mean square (RMS) error is $\sqrt{\varepsilon^2/(M-1)} = 0.4$ dB. The maximum phase drift range among elements is 6.3°.

In the phase control accuracy measurement, the attenuation

0018-9456 (c) 2020 IEEE. Personal use is permitted, but republication/redistribution requires IEEE permission. See http://www.ieee.org/publications_standards/publications/rights/index.html for more information.
Authorized licensed use limited to: Aalborg Universitetsbibliotek. Downloaded on October 01,2020 at 12:59:20 UTC from IEEE Xplore. Restrictions apply.

This article has been accepted for publication in a future issue of this journal, but has not been fully edited. Content may change prior to final publication. Citation information: DOI 10.1109/TIM.2020.3024428, IEEE Transactions on Instrumentation and Measurement

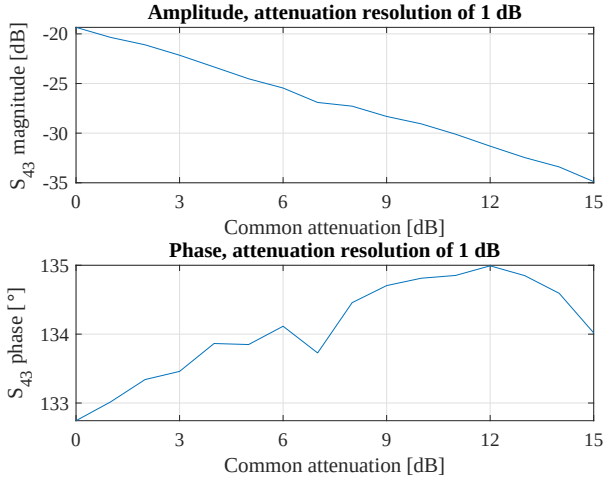

Fig. 12. Complex S_{43} as a function of the common attenuation in the "all-on" mode.

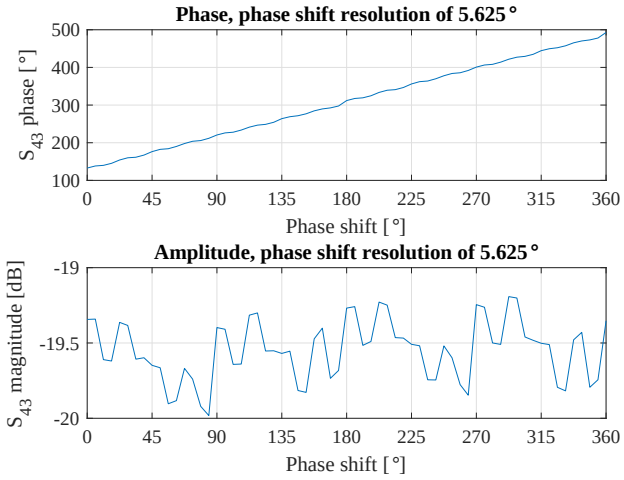

Fig. 13. Complex S_{43} as a function of the phase shift in the "all-on" mode.

of the selected element is set to 0 dB. The phase shift is swept from 0° to 360° with a resolution step of 5.625° (i.e. a total of 65 measurements for $M = 65$ phase shift values). Fig. 11 gives the complex S_{43} as a function of phase shift. The phase rotates while the amplitude fluctuates with the phase shifted. Similarly, the phase control error $\varepsilon = x - a$ is defined to be the relative deviation of measured S_{43} phase increment x between every two adjacent phase shift values with respect to the phase setting offset $a = 5.625°$. The maximum error range among elements and the corresponding RMS error are $[-3.7°, 14.4°]$ and 2.4°, respectively. The maximum amplitude fluctuation range among elements is 1.2 dB.

Note that the complex S_{43} has different values for 16 elements without attenuation and phase shift. It is because of the initial excitations differences of elements, which can be indicated in the following measurement of array calibration.

2) "All-on" Mode: All elements are enabled in the "all-on" mode. In the gain control accuracy measurement, the attenuation and the phase shift of each element is set to 0 dB and 0°, respectively. The attenuation of common attenuators is swept from 0 to 15 dB with a resolution step of 1 dB ($M = 16$ and $a = -1$ dB). The complex S_{43} over the common attenuation is displayed in Fig. 12. The error range of gain control and the corresponding RMS error are $[-0.5, 0.6]$ dB and 0.3 dB, respectively. The phase drift range is 2.2°.

The attenuation of all elements is set to 0 dB in the phase control accuracy measurement. The phase shift of all elements is swept from 0° to 360° with a resolution step of 5.625° ($M = 65$ and $a = 5.625°$). The complex S_{43} is given in Fig. 13 as a function of the phase shift. The error range of phase control and the corresponding RMS error are $[-4.2°, 9.2°]$ and 2.8°, respectively. The amplitude variation range is 0.8 dB.

Control accuracy differs in the "on-off" mode and "all-on" mode. The "all-on" mode basically has better accuracy than the "on-off" mode. It might be due to the superposition effect of the "all-on" mode, so that the overall error remains small even though the single element has large control error. AiP might be applied for various scenarios, where amplitude excitation of elements are different. For example, for beamforming application, all elements are enabled with equal gain, while for tapering algorithms, some elements might be attenuated. Therefore, it is important to understand the control accuracy of various AiP settings. This is largely overlooked in the literature, and a new finding in our measurement campaign.

C. Array Calibration

The AiP calibration measurements are conducted over the air in this part. The measurements of three calibration methods are investigated and their calibration results are compared. Finally, the feasibility of rotating-element electric-field vector (REV) [19]–[21] calibration measurement is validated on the AiP experimental platform.

1) Comparison of Calibration Methods: First, we investigate three calibration methods: "on-off" calibration, "inverse" calibration, and REV calibration. The "on-off" method is to sequentially enable one element each time, and to measure the complex S_{43} for each element, finally to obtain the relative complex excitation of elements. To evaluate the AiP element branch inhomogeneities, a ground-truth measurement is basically required to obtain the "ground-truth" of the AiP element excitations. The "on-off" method is always considered to be the ground-truth measurement in sub-6 GHz, e.g. in [22]. For this reason, the ground-truth "on-off" measurement is usually used as a comparison target (i.e. reference measurement) to validate other calibration measurement methods. In "inverse" method, all elements are excited simultaneously in the measurement. Two measurements of the complex S_{43} are required for each element. The first and the second measurements are performed before and after the phase inversion of each element, respectively. The complex excitation of each element is derived by comparing the two measured complex values. The above two methods are both based on the complex signal measurement. In the REV method, all elements are active and the phase of one element is tuned from 0° to 360° each time, while other elements stay unchanged. Different from the

0018-9456 (c) 2020 IEEE. Personal use is permitted, but republication/redistribution requires IEEE permission. See http://www.ieee.org/publications_standards/publications/rights/index.html for more information.
Authorized licensed use limited to: Aalborg Universitetsbibliotek. Downloaded on October 01,2020 at 12:59:20 UTC from IEEE Xplore. Restrictions apply.

This article has been accepted for publication in a future issue of this journal, but has not been fully edited. Content may change prior to final publication. Citation information: DOI 10.1109/TIM.2020.3024428, IEEE Transactions on Instrumentation and Measurement

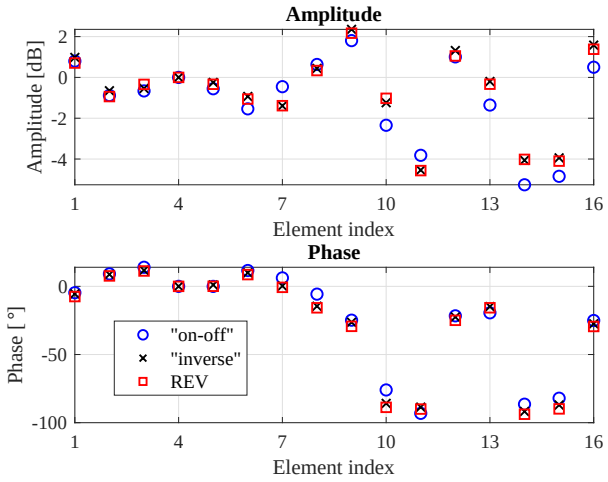

Fig. 14. AiP calibration results using three calibration methods.

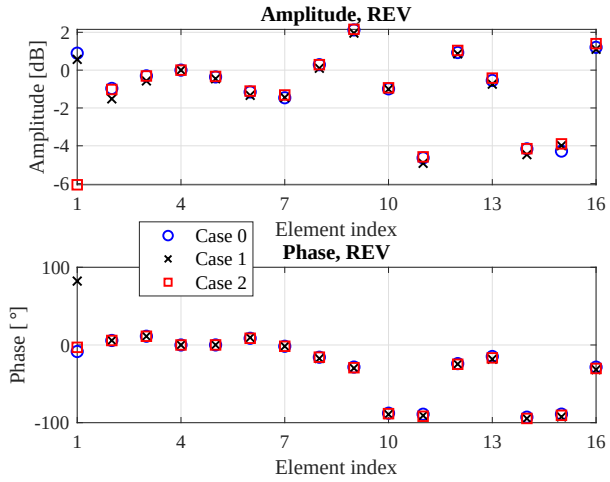

Fig. 15. Calibration results using REV method in three Cases.

"inverse" method, the REV method is based on amplitude-only measurement.

Fig. 14 depicts the calibration results using above three methods with 0 dB and 0° set for all elements. The "inverse" and REV methods have the similar calibration results, whereas the results of the "on-off" method are different from those. The degree of difference depends on the AiP design and antenna coupling. Weaker antenna coupling leads to less difference. In case that the antenna coupling is considerable and cannot be ignored with all elements active, the "on-off" method is not suitable as a reference for the situation in which all elements are active (e.g. the REV method). Instead, the "inverse" method can be a reference of the REV method. It is emphasized that the "on-off" method is typically used as the reference for other methods. Our analysis showed that the "on-off" method is not necessarily a good choice, especially for mmWave AiP.

Since the mutual coupling effect is essential for mmWave phased array calibration, the calibration is required to be conducted with all elements enabled. Moreover, the REV calibration measurement based on amplitude-only measurement is more promising in comparison with the complex measurement due to the large measurement error of phase for mmWave measurement. In the following, the REV calibration measurements are further conducted.

2) REV Calibration Validation: To further demonstrate the effectiveness of REV calibration measurement, the calibration results of the REV measurement are compared among different sets of initial excitations of elements. One is when the initial attenuation and phase shift of the first element are set to 0 dB and 90°, respectively (denoted as Case 1 in the following). The other is when the initial attenuation and phase shift of the first element are set to 7 dB and 0°, respectively (denoted as Case 2 in the following). In these two cases, other elements are set with 0 dB and 0°. The reference case is that the initial attenuation and phase shift of all elements are set to 0 dB and 0°, respectively (denoted as Case 0 in the following). Fig. 15 demonstrates the calibration results of REV measurement for Cases 0, 1 and 2. A phase difference of 90.6° between Cases 0 and 1 is distinguished in the first element (0.6° error relative to 90°), whereas the amplitude is the same for all elements within a error range of ± 0.4 dB. An amplitude difference of -7.0 dB between Cases 0 and 2 is distinguished in the first element (0 dB error relative to -7 dB), while the phase is the same for all elements within a error range of $\pm 3.7°$. It indicates that the difference of calibration results among three Cases are distinguished well and the REV calibration measurement has good accuracy.

D. Beam Steering

The S_{43} amplitude is measured in the broadside direction of AiP when the main beam is steered. The measured amplitude at different main beam tilting angles (defined as the beam-steering pattern for an electronic-steered AiP array) is investigated in the following. As mentioned in the previous section, the relative initial excitations of the AiP elements are obtained after the REV calibration measurement. The differences among initial excitations of elements are calibrated by attenuators and phase shifters so that the amplitude and phase of the excitations are aligned in the allowed error range. After the REV calibration, the beam steering operation is performed and the beam-steering pattern is measured. The measured beam-steering patterns before and after calibration are drawn in Fig. 16 for the backward and forward tilting as an example. As the main beam is electrically steered, the nulls and sidelobes of the radiation pattern are turned to the broadside direction of AiP. Once the AiP array is calibrated well, the nulls of radiation pattern are deeper, and the radiation pattern of AiP array is considered to be the same at a fixed and the same tilting angle for backward and forward tilting. For this reason, the null of beam-steering pattern would be deeper as well, and the beam-steering pattern would be more symmetric with respect to the broadside direction of AiP (denoted as tilting angle 0°) after AiP calibration. Fig. 16 shows that the null depth levels obtained after calibration are lower than those before calibration, as expected. Also, the

0018-9456 (c) 2020 IEEE. Personal use is permitted, but republication/redistribution requires IEEE permission. See http://www.ieee.org/publications_standards/publications/rights/index.html for more information.
Authorized licensed use limited to: Aalborg Universitetsbibliotek. Downloaded on October 01,2020 at 12:59:20 UTC from IEEE Xplore. Restrictions apply.

This article has been accepted for publication in a future issue of this journal, but has not been fully edited. Content may change prior to final publication. Citation information: DOI 10.1109/TIM.2020.3024428, IEEE Transactions on Instrumentation and Measurement

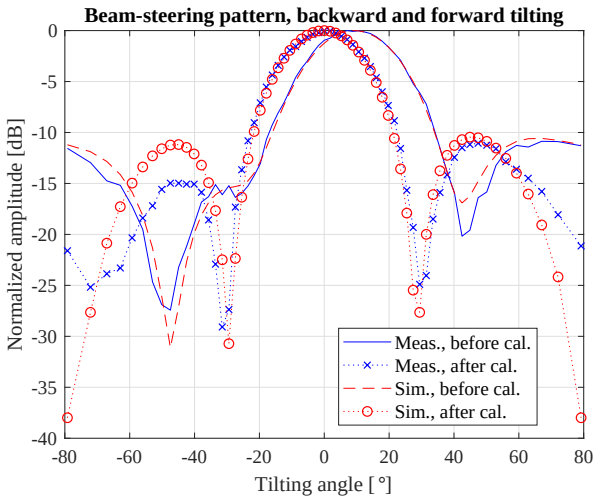

Fig. 16. Measured and simulated beam-steering patterns before and after REV calibration for the backward and forward tilting. The backward and forward tilting angles are denoted by negative and positive angles, respectively.

sidelobes are more symmetrical with respect to the main beam after calibration. Therefore, we can examine the effectiveness of AiP calibration from checking the beam-steering patterns before and after array calibration, without the need for radiation pattern measurement. In addition, the main beam of beam-steering pattern is aligned to the broadside direction of AiP after array calibration. This also reflects the influence of array calibration on the main beam of radiation pattern.

It is worth emphasizing that the null depth levels have a ideal minimum and the sidelobes are completely symmetrical after an ideal calibration. Because of the control error of attenuators and phase shifters, however, the amplitude and phase of the element excitations are not completely aligned after practical calibration. Taking into account the control error of attenuators and phase shifters, corresponding simulations are performed based on the obtained element excitations to validate the measured results, as depicted in Fig. 16. The measured results match well with the simulated ones in the main lobe for both before and after calibration, though slight deviation exists in terms of null depth and sidelobes. The difference between measured and simulated patterns might come from the element patterns (the isotropic element patterns are assumed in the simulation since the practical element patterns are unknown.)

Note that the pattern is improved after the calibration on condition that the control error of attenuators and phase shifters is less than the differences among initial complex excitations of elements. The improvement is more significant for smaller control error. Otherwise, little difference might exist between patterns before and after calibration.

V. Conclusion

An efficient and automated mmWave phased array AiP experimental platform is proposed in this paper. The platform is validated experimentally based on several measurement campaigns. The platform has complete functions and strong flexibility, avoiding the heavy workload of controlling the AiP. Combining programmable measurement instruments, the experimental platform can accomplish extensive measurement work efficiently. It takes 0.7 s in total for the experimental platform to complete one combination operation for the status update of AiP, S-parameter measurement, and data saving.

In the performance evaluation of the experimental platform, customized temperature compensation strategy based on amplitude monitoring is proposed and validated. The proposed strategy offers more stable temperature stability results. The control error of the AiP experimental platform depends on the status of AiP elements. In the "on-off" mode, the gain and phase control error range are $[-0.4, 1.2]$ dB and $[-3.7°, 14.4°]$, respectively. While in the "all-on" mode, the gain and phase control error range are $[-0.5, 0.6]$ dB and $[-4.2°, 9.2°]$, respectively. In AiP calibration, the "on-off" and "all-on" modes will present different calibration results. The "on-off" method in the "all-on" mode, typically used in the literature as a reference in the sub-6 GHz, is not necessarily a good way to calibrate the mmWave AiP. Calibration methods in the "all-on" mode are of significant importance for the improvement of side-lobes and nulls in applications of mmWave base stations.

As a future work one could validate some algorithms developed for mmWave applications based on the AiP experimental platform, e.g. array calibration, array fault element detection, array pattern reconstruction, plane wave generators, etc.

References

[1] E. Hossain and M. Hasan, "5G cellular: key enabling technologies and research challenges," *IEEE Instrumentation and Measurement Magazine*, vol. 18, no. 3, pp. 11–21, June 2015.

[2] M. Zhong, Y. Yang, H. Yao, X. Fu, O. A. Dobre, and O. Postolache, "5G and IoT: Towards a new era of communications and measurements," *IEEE Instrumentation and Measurement Magazine*, vol. 22, no. 6, pp. 18–26, Dec. 2019.

[3] U. R. Pfeiffer, J. Grzyb, D. Liu, B. Gaucher, T. Beukema, B. A. Floyd, and S. K. Reynolds, "A chip-scale packaging technology for 60-GHz wireless chipsets," *IEEE Transactions on Microwave Theory and Techniques*, vol. 54, no. 8, pp. 3387-3397, Aug. 2006.

[4] Y. P. Zhang and D. Liu, "Antenna-on-Chip and Antenna-in-Package Solutions to Highly Integrated Millimeter-Wave Devices for Wireless Communications," *IEEE Transactions on Antennas and Propagation*, vol. 57, no. 10, pp. 2830–2841, Oct. 2009.

[5] D. Liu, X. Gu, C. W. Baks, and A. Valdes-Garcia, "Antenna-in-Package Design Considerations for Ka-Band 5G Communication Applications," *IEEE Transactions on Antennas and Propagation*, vol. 65, no. 12, pp. 6372–6379, Dec. 2017.

[6] Y. Zhang and J. Mao, "An Overview of the Development of Antenna-in-Package Technology for Highly Integrated Wireless Devices," *Proceedings of the IEEE*, vol. 107, no. 11, pp. 2265–2280, Nov. 2019.

[7] A. Valdes-Garcia, B. Sadhu, X. Gu, Y. Tousi, D. Liu, S. K. Reynolds, J. Haillin, S. Sahl, and L. Rexberg, "Circuit and antenna-in-package innovations for scaled mmWave 5G phased array modules," *2018 IEEE Custom Integrated Circuits Conference (CICC)*, April 2018.

[8] B. Sadhu, Y. Tousi, J. Hallin, S. Sahl, S. K. Reynolds, et al. "A 28-GHz 32-Element TRX Phased-Array IC With Concurrent Dual-Polarized Operation and Orthogonal Phase and Gain Control for 5G Communications," *IEEE Journal of Solid-State Circuits*, vol. 52, no. 12, pp. 3373–3391, Dec. 2017.

[9] J. Park, D. Choi, and W. Hong, "Millimeter-Wave Phased-Array Antenna-in-Package (AiP) Using Stamped Metal Process for Enhanced Heat Dissipation," *IEEE Antennas and Wireless Propagation Letters*, vol. 18, no. 11, pp. 2355–2359, November 2019.

[10] Y. Wang, H.-C. Huang, Z. Zhu, X. Jian, and R. Ma, "A Miniaturized Wideband Dual-Polarized 5G mm-Wave Antenna-in-Package (AiP) Array for Cellular Phones," *2019 International Symposium on Antennas and Propagation (ISAP)*, Oct. 2019.

0018-9456 (c) 2020 IEEE. Personal use is permitted, but republication/redistribution requires IEEE permission. See http://www.ieee.org/publications_standards/publications/rights/index.html for more information.
Authorized licensed use limited to: Aalborg Universitetsbibliotek. Downloaded on October 01,2020 at 12:59:20 UTC from IEEE Xplore. Restrictions apply.

This article has been accepted for publication in a future issue of this journal, but has not been fully edited. Content may change prior to final publication. Citation information: DOI 10.1109/TIM.2020.3024428, IEEE Transactions on Instrumentation and Measurement

[11] I. Nasr, R. Jungmaier, A. Baheti, D. Noppeney, J. S. Bal, M. Wojnowski, E. Karagozler, H. Raja, J. Lien, I. Poupyrev, and S. Trotta, "A Highly Integrated 60 GHz 6-Channel Transceiver With Antenna in Package for Smart Sensing and Short-Range Communications," *IEEE Journal of Solid-State Circuits*, vol. 51, no. 9, pp. 2066–2076, Sept. 2016.

[12] Y. Zhang, "Antenna-in-Package Technology: Its Early Development," *IEEE Antennas and Propagation Magazine*, vol. 61, no. 3, pp. 111–118, June 2019.

[13] Z. Wang, L. Mao, and R. Liu, "High-Accuracy Amplitude and Phase Measurements for Low-Level RF Systems," *IEEE Transactions on Instrumentation and Measurement*, vol. 61, no. 4, pp. 912–921, April 2012.

[14] G. Barchi, D. Fontanelli, D. Macii, and D. Petri, "On the Accuracy of Phasor Angle Measurements in Power Networks," *IEEE Transactions on Instrumentation and Measurement*, vol. 64, no. 5, pp. 1129–1139, May 2015.

[15] M. A. Salas-Natera, R. M. Rodriguez-Osorio, and L. de Haro, "Procedure for Measurement, Characterization, and Calibration of Active Antenna Arrays," *IEEE Transactions on Instrumentation and Measurement*, vol. 62, no. 2, pp. 377–391, Feb. 2013.

[16] Comprehensive Survey of Commercial mmWave Phased Array Companies. https://www.microwavejournal.com/articles/33357-comprehensive-survey-of-commercial-mmwave-phased-array-companies.

[17] Amotech Co., Ltd. http://global.amotech.co.kr.

[18] AWMF-0158 28 GHz Silicon 5G Tx/Rx Quad Core IC, Anokiwave Inc. https://www.anokiwave.com/products/awmf-0158/index.html.

[19] S. Mano and T. Katagi, "A method for measuring amplitude and phase of each radiating element of a phased array antenna," *Trans. IECE*, vol. J65-B, no. 5, pp. 555–560, May 1982.

[20] T. Takahashi, Y. Konishi, and I. Chiba, "A Novel Amplitude-Only Measurement Method to Determine Element Fields in Phased Arrays," *IEEE Transactions on Antennas and Propagation*, vol. 60, no. 7, pp. 3222–3230, July 2012.

[21] R. Long, J. Ouyang, F. Yang, W. Han, and L. Zhou, "Fast Amplitude-Only Measurement Method for Phased Array Calibration," *IEEE Transactions on Antennas and Propagation*, vol. 65, no. 4, pp. 1815–1822, April 2017.

[22] F. Zhang, W. Fan, Z. Wang, Y. Zhang and G. F. Pedersen, "Improved Over-the-Air Phased Array Calibration Based on Measured Complex Array Signals," *IEEE Antennas and Wireless Propagation Letters*, vol. 18, no. 6, pp. 1174–1178, June 2019.

0018-9456 (c) 2020 IEEE. Personal use is permitted, but republication/redistribution requires IEEE permission. See http://www.ieee.org/publications_standards/publications/rights/index.html for more information.
Authorized licensed use limited to: Aalborg Universitetsbibliotek. Downloaded on October 01,2020 at 12:59:20 UTC from IEEE Xplore. Restrictions apply.